

RSC Advances



This is an *Accepted Manuscript*, which has been through the Royal Society of Chemistry peer review process and has been accepted for publication.

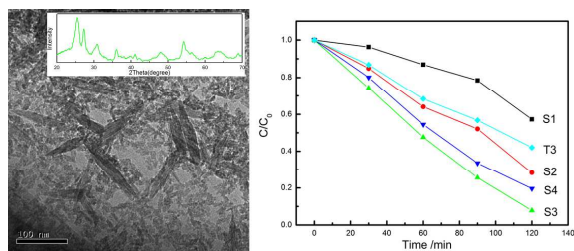
Accepted Manuscripts are published online shortly after acceptance, before technical editing, formatting and proof reading. Using this free service, authors can make their results available to the community, in citable form, before we publish the edited article. This *Accepted Manuscript* will be replaced by the edited, formatted and paginated article as soon as this is available.

You can find more information about *Accepted Manuscripts* in the [Information for Authors](#).

Please note that technical editing may introduce minor changes to the text and/or graphics, which may alter content. The journal's standard [Terms & Conditions](#) and the [Ethical guidelines](#) still apply. In no event shall the Royal Society of Chemistry be held responsible for any errors or omissions in this *Accepted Manuscript* or any consequences arising from the use of any information it contains.

Graphical and textual abstract

TiO₂-based nanomaterials could reach the maximal photoactivity when designing 0D/1D heterogenous structure with appropriate phase composition and high surface area.



Cite this: DOI: 10.1039/c0xx00000x

www.rsc.org/xxxxxx

ARTICLE TYPE

Effect of phase composition, morphology, and specific surface area on the photocatalytic activity of TiO₂ nanomaterials

Hao Cheng^b, Jingyu Wang^{a,b,*}, Yizhi Zhao^b, Xijiang Han^{b,*}*Received (in XXX, XXX) Xth XXXXXXXXXX 20XX, Accepted Xth XXXXXXXXXX 20XX*

DOI: 10.1039/b000000x

The synergistic effect between anatase and rutile TiO₂ particles for photocatalysis has been widely reported. Besides the phase composition, both morphology and specific surface area play important roles in affecting the photocatalytic activity of TiO₂-based materials. However, comprehensive study of the effects of these properties is missing so far. Using a facile soft-chemical strategy, we synthesize a series of TiO₂ samples with desired phase composition, morphology, specific surface area, but otherwise identical properties. The correlation of these properties to the photoreactivity is investigated by degrading three typical dye molecules. The composite with anatase-to-rutile ratio as 7:3 displays optimal results. Meanwhile, we find an interlaced influence of morphology and specific surface area. The superior activity is achieved in 0D/1D TiO₂ heterogenous composite even it possesses much lower surface area than pure 0D particles. We proposed that the improvement is due to the combined effect of higher surface-to-volume ratio of 0D particles and lower carrier recombination rate of 1D nanorods. In this way, TiO₂-based materials could reach the maximal photocatalytic performance if designing 0D/1D heterogenous structure with appropriate phase composition and high specific surface area.

Introduction

Titanium dioxide, TiO₂, as an n-type semiconductor takes the advantage of low cost, nontoxicity, chemical/photo-stability, and strong oxidizing power.¹⁻³ Since the discovery of photoelectrochemical splitting of water on n-TiO₂ electrodes,⁴ TiO₂-mediated heterogeneous photocatalysis has attracted extensive interest because of its potential applications to environmental purification and energy conversion. TiO₂ has three main crystalline phases: brookite (B), anatase (A), and rutile (R). A is generally considered to be the most photocatalytically active due to its higher adsorption affinity for organic molecules and a lower recombination rate.⁵⁻⁷ There are plenty of experimental evidences that reveal the better photocatalytic performance of A/R composites than any single component.⁸⁻¹³ It should be noted that A and R have the same fundamental structural octahedral units (TiO₆), but the octahedral units' edges and corners sharing in different manners.¹⁴ In comparison to other coupled semiconductor systems, the A/R TiO₂ heterogeneous nanostructure is intriguing because it involves only a change in the crystal structure and can be achieved in the same solution.^{15,16}

It is believed that a synergistic effect between the two phases significantly enhances the photocatalytic property of TiO₂. The photogenerated electrons could transfer from one phase to another, which has slightly lower conduction band energy, and thus the charge recombination can be suppressed. Through studying the samples with varying phase composition, some groups have demonstrated the existence of synergetic effect in case of the anatase content ranging from ~20% to ~90%.¹⁷⁻²² As

a result, engineering the phase composition has gradually been recognized as a promising methodology to improve the photocatalytic activity of TiO₂.

Besides the significant influence of phase composition, morphology will also play a great role on the physical/chemical properties of materials.^{9,23-25} For TiO₂, spherical nanoparticles give higher surface-to-volume ratio than one-dimensional (1D) materials such as nanorods, nanowires, and nanotubes. However, the photoinduced charge carrier recombination at surface trapping sites is increased in spherical particles smaller than a certain dimension (about 10 nm), leading to lower photocatalytic quantum yields.^{26,27} Because of the delocalization of charge carriers, the high transfer rate of electrons can be achieved in one-dimensional materials.

In addition, most heterogeneous catalysis between the catalysts and reactants occurs on the surface or at the interface, so the efficiency partly depends on the specific surface area of materials. Large surface area will provide more active sites to not only react with absorbed water and hydroxyl to form important oxidative hydroxyl radicals but also anchor organic molecules for photodegradation.²⁸⁻³⁰ Generally, the specific surface area and surface-to-volume ratio dramatically increase with the decrease of crystal size. In this regard, small spherical particles may possess higher surface area than nanorods or nanowires with relatively large size in one dimension.

Actually, the effect of physical/chemical properties on the overall efficiency of TiO₂ photocatalytic system is complicated, which is dependent not only on the above three points, but also on other factors, such as degree of crystallinity, surface

cleanliness, defect density, and so on. Although these factors are known to affect the photocatalytic performance of TiO₂ from different angles, there is few systematical and detailed discussions covering all of them. Several approaches have been reported to engineering the phase composition of TiO₂, such as directly mixing A and R together, annealing at different temperature, and introducing additives in crystallization process.⁸ However, the synergetic effect is often not observed in simple mixture of A and R due to poor contact between the two phases.^{31,32} Altering annealing temperature causes the obvious changes in crystallinity, particle size, and surface area besides the A/R ratio.^{10,33,34} Additives bring about undesired impurities on the surface or in the crystal lattice with varying kinds or concentrations, which influence the surface cleanliness and defect density.^{21,22} In light of the well-established methodology in our previous works,^{15,16,35} a facile soft-chemical strategy is applied to this work. TiO₂ samples with different phase compositions are synthesized by simply adjusting the volume of peptizing agent, while the concentration of medium, peptization time, and reaction temperature are kept constant. In this way, the influence on crystallinity, surface cleanliness, and defect density can be negligible. As mentioned above, the morphology and specific surface area of photocatalysts always have an interlaced influence on their performance. Therefore, in order to maximize the photoactivity, comprehensive roles of phase composition, morphology, and specific surface area need to be taken into account.

Experiment section

Materials synthesis

All of the chemical reagents used in the experiment were of analytical grade. Typical synthetic procedure of TiO₂ samples under alkaline condition was as follows:^{15,16} 9 mL tetra-*n*-butyl titanate was mixed with 66 mL absolute ethanol to form homogeneous solution. Then it was added dropwise into 80 mL distilled water slowly under magnetic stirring for about 40 min. An opaque white suspension was released as consequence of hydrolysis of precursor. Subsequently, the suspension was heated at 70 °C in a three-neck flask under magnetic stirring for approximate 2 h to form smooth slurry. This step is to guarantee the complete hydrolysis of precursor and condensation of suspension. After adding 300 mL 1 M NaOH aqueous solution, the mixture was stirring for 24 h. In the next stage, the resulting intermediate product was harvested by centrifugation, followed by washing with distilled water for several times until it reached neutral. Then the intermediate product was divided into eight equipotent portion for parallel experiments. Each portion was dissolved in a certain volume of 1 M HNO₃ (20 mL, 60 mL, 80 mL, 120 mL, were denoted as S-series samples, from S1 to S4, respectively). The resulting solution was stirred for 4 h at 70 °C. After centrifugation, the precipitation was re-dispersed in distilled water and existed as stable hydrosol. Finally, the hydrosol was dried at room temperature by air blowing to obtain the TiO₂ powder.

For comparison, TiO₂ powder was synthesized without treating by 1 M NaOH solution.³⁵ The rest processes were kept the same. 9 mL tetra-*n*-butyl titanate was mixed with 66 mL absolute

ethanol to form homogeneous solution. Then it was divided into four parts and underwent the following process. Instead of adding NaOH aqueous solution, the condensed suspension was directly dissolved in a certain volume of 1 M HNO₃ solution (60 mL, 110 mL, 180 mL). After stirring for 4 h at 70 °C and centrifugation, the precipitation was re-dispersed in distilled water and dried by air blowing. The as-obtained samples were labeled as T-series samples (T1, T2, and T3, respectively). Anatase nanoparticles with an average particle size of ~20 nm, which are prepared in light of the literature, are used as reference sample (Ref.).³⁶

Characterization

X-ray powder diffraction (XRD) patterns were obtained using a Shimadzu XRD-6000 diffractometer using Cu K α radiation, λ_{Cu} =0.15418 nm. Scanning rate was 10° per minute, ranging from 20° to 70°. Working volt was 40 kV, and working current was 30 mA. Transmission electron microscopy (TEM) images were obtained using an FEI Tecnai G2 T20 S-Twin microscope with an accelerating voltage of 200 kV (FEI, USA). The samples for TEM were prepared by dispersing the sol products in ethanol; the dispersion was then dropped on carbon copper grids. The grids were left for a few minutes to let the solvent evaporate. Raman spectra were collected on a Thermo Fisher DXR smart Raman spectrometer over a range from 100 cm⁻¹ to 2000 cm⁻¹. The incident laser power was kept at 10 mW, and total accumulation time was 2 s. Nitrogen adsorption and desorption isotherms were conducted at 77 K on Micrometrics ASAP2000 system using the Brunauer–Emmett–Teller (BET) method. Photoluminescence (PL) spectra were measured at room temperature on a PerkinElmer LS55. The excitation wavelength was 335 nm, with a scanning speed of 1000 nm min⁻¹. The width of the excitation slit was 4 nm and that of emission slit was 15 nm.

Photocatalytic activity test

Photocatalytic activities of as-prepared samples were measured by degrading aqueous solutions of methylene blue (MB), methyl orange (MO), acridine orange (AO), and 2,4-dichlorophenol (2,4-DCP) under UV light irradiation. In a typical performance, 10 mg sample was added into 10 mL distilled water and then the mixture was processed by ultrasonication to get a uniform suspension. After that 20 μ L 1 M HCl aqueous solution and certain volume (40 μ L, 80 μ L, 120 μ L for MB, MO, AO, separately) of dye aqueous solution of 0.2 wt% were added into the suspension. In the photoreaction with colorless organic pollutant, 120 μ L 0.2 wt% 2,4-DCP was added into the suspension. A high-pressure 120 W mercury (Hg) lamp (main wavelength 365 nm) was used as light source. Before irradiation, the suspensions were stirred for about 40 min in the darkness to establish adsorption–desorption equilibrium. At given time intervals, 800 μ L of the suspension was sampled and centrifuged to remove remnant photocatalyst. Supernatant was subsequently analyzed by recording absorption spectra of dyes using a TU 1901 ultraviolet visible spectrophotometer (Persee, Inc. Beijing). Changes of maximum absorption (664 nm for MB, 506 nm for MO, 468 nm for AO, and 284 nm for 2,4-DCP) were obtained, which reflected the decrease of dye concentration.

Results and discussion

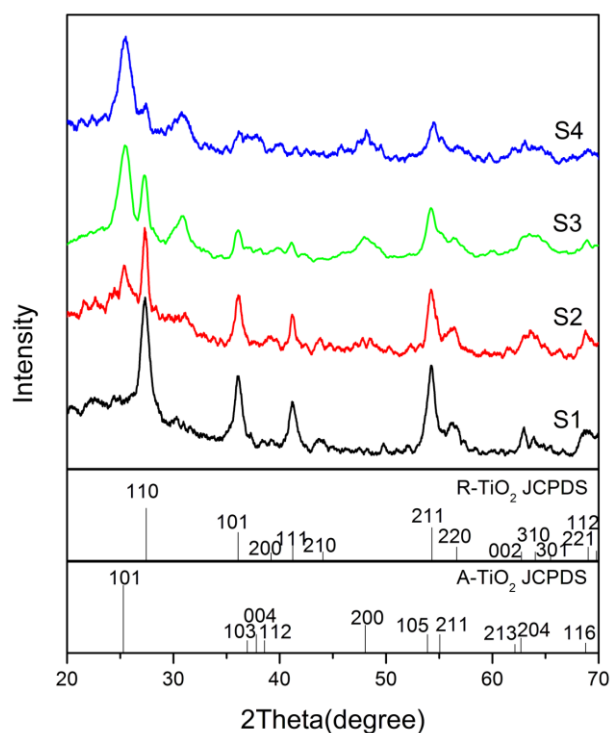


Figure 1 XRD patterns of samples obtained from different volume of 1 M HNO₃. The vertical lines indicate the position and intensity of A and R reflections (JCPDS 21-1272 and 21-1276).

5 Effect of acid volume on phase composition, morphology, and specific surface area of TiO₂

In order to avoid the influence of some other factors on the photocatalytic performance of TiO₂ samples, the kind as well as concentration of additives, peptization time, and reaction temperature are kept constant in the whole preparation process. Through varying the volume of peptizing agent, HNO₃ aqueous solution, we have prepared four typical samples that contain different values of A-to-R ratio. XRD patterns of these four samples are given in Fig. 1. The phase composition of the samples can be estimated from the respective XRD peak intensities using the following equation³⁷

$$f_A = \frac{1}{1 + \frac{I_R}{K I_A}}$$

$$K = 0.68, f_A \leq 0.2; K = 0.79, f_A > 0.2$$

where f_A is the weight fraction of A in the powder, I_A and I_R are the X-ray intensities of the A(101) and R(110) diffraction peaks, respectively. The results are given in Table 1. The sample S1 consists of pure R phase, while the others are composites of A and R. The weight fraction of A rises with the increased volume of acid medium, whereas that of R declines, indicating that large space for particles dispersion or movement is more favorable for the formation and stabilization of A phase. As reported in our previous study, the intermediate product generated by NaOH treatment is lamellar protonated titanate (LPT, H₂Ti₅O₁₁•3H₂O).³⁸ Because of the high similarity in crystal structure between them, LPT transforms into A phase in a rapid and complete manner. According to the dissolution-reassembly mechanism, the movement and collision of crystal particles in the system have

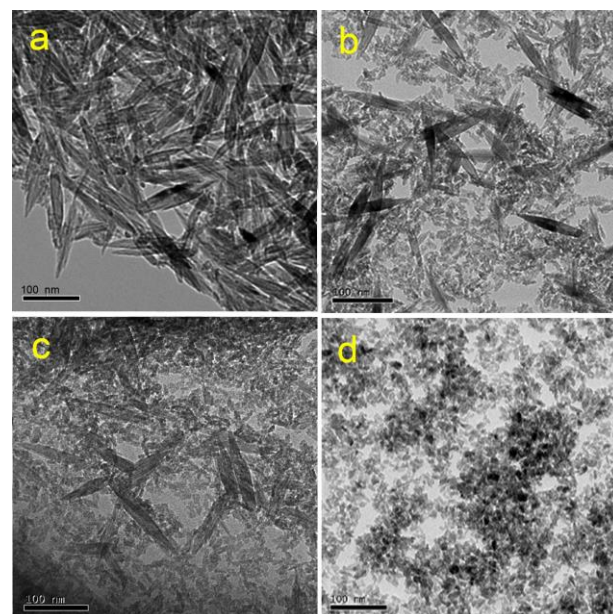


Figure 2 TEM images of samples. (a) S1, (b) S2, (c) S3, (d) S4.

crucial impacts on the arrangement and packing of structural units and thus affect phase composition and morphology.¹⁵ It is known that A and R consist of the same fundamental structural unit, but the structure of R crystals with two-edge sharing and a linear chain is more compact than that of A crystals. A crystals have four-edge sharing and zigzag chain, which require more space. Penn et al. reported that the A-to-R transition was initiated from the oriented contacts between A particles.³⁹ In case of relatively small volume of HNO₃ medium, the particles disperse in a limited space, which facilitates the orientational aggregation and promotes the A-to-R phase transition. With increasing the volume, the lack of proper attachment or coordination of A particles might reduce the possibility of R nucleation. Such evolution of crystal phase and morphology is clearly illustrated with TEM observations (Fig. 2a-d). As shown in Fig. 2a, the growth of R during acid peptization is oriented to the formation of elongated nanorod. Different from the 1D shuttle-like R nanorod (Nr), Fig. 2b-d show that anatase crystal is displayed in 0D nanoparticle (Np). Both of Nr and Np are highly dispersed and uniformly controlled. If hindering the A-to-R phase transition by increasing the medium volume, both the fraction of R and the average size of crystals decrease. The gradual decrease of the crystal size also suggests the decrease of aggregation degree. From S1 to S4, morphologies of the as-prepared samples change from almost Nr, Nr-dominated composite, Np-dominated composite, to almost Np, along with the changes in crystal phase from pure R to A. Notably, A is the stable phase when the particle size is smaller than the critical size (~16 nm) because of its lower surface energy with respect to R.⁴⁰ This can also explain why it is hard to form R in large volume of HNO₃ medium.

The A and R phases of TiO₂ can be sensitively identified by Raman spectroscopy (Fig. 3). Anatase gives characteristic scatterings at 152, 208, 414, 512, 515 (superimposed with the 512 cm⁻¹ band), and 632 cm⁻¹, which are attributed to the Eg, Eg, B1g, A1g, B1g, Eg, respectively. The rutile shows major Raman bands at 151 (superimposed with the band of anatase phase), 247, 445, and 612 cm⁻¹, which are assigned to the B1g, two-phonon

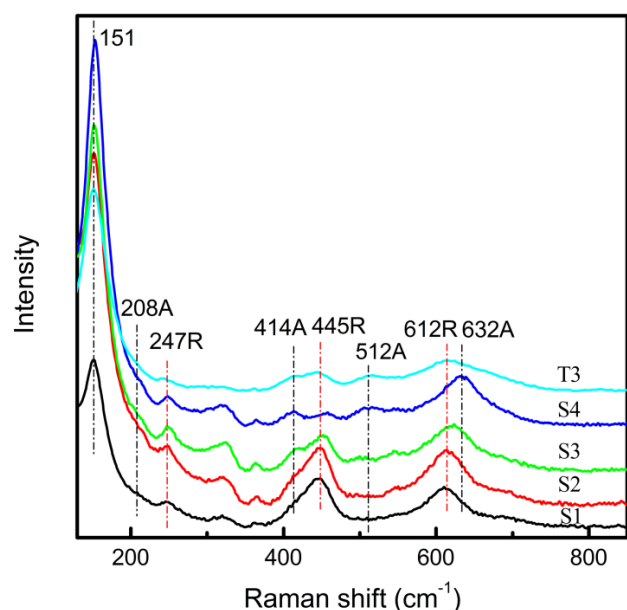


Figure 3 Raman spectra of samples obtained from different experiment conditions. Samples from S1 to S4 represent the different volume of HNO₃ peptizer after NaOH treatment. T3 represents the sample without NaOH treatment.

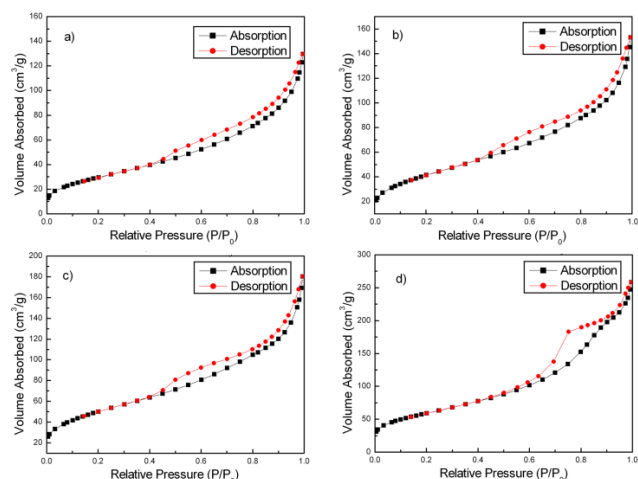


Figure 4 Nitrogen adsorption-desorption isotherms of samples. (a) S1, (b) S2, (c) S3, (d) S4.

scattering, Eg, A1g, respectively.⁴¹ It should be mentioned that the intensity of band at 151 or 152 cm⁻¹ was quite different for the two phases. It is the strongest one for the anatase phase and the

Table 1 Experimental conditions and properties of as-prepared TiO₂ samples.

Sample	S-series (treating by NaOH)				T-series (not treating by NaOH)		
	S1	S2	S3	S4	T1	T2	T3
Amount of intermediate product	1/8	1/8	1/8	1/8	1/4	1/4	1/4
Volume of HNO ₃ medium (mL)	20	60	90	120	60	110	180
Weight fraction of A (%)	≈0	34	70	88	≈0	31	71
Weight fraction of R (%)	≈100	66	30	12	≈100	69	29
Average size, perpendicular to (101) for A and (110) for R	13.4 nm (R)	8.2 nm (A) 11.0 nm (R)	5.5 nm (A) 11.0 nm (R)	5.3 nm (A) -	- 12.3 nm (R)	7.3 nm (A) 14.6 nm (R)	4.1 nm (A) 11.0 nm (R)
Specific surface area (S _{BET} , m ² /g)	111	153	184	215	127	176	235
Morphology	almost Nr	Np+Nr	Np+Nr	almost Np	Np	Np	Np

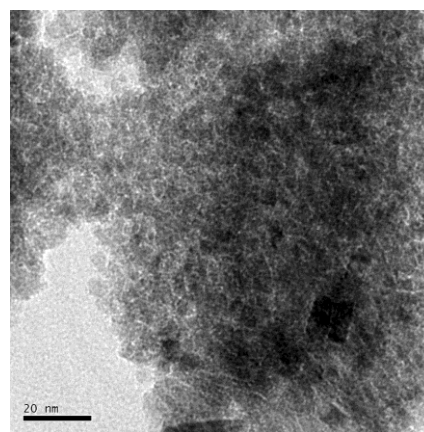


Figure 5 TEM images of T3 (one of T-series samples with no NaOH treatment, possessing similar phase composition to S3).

weakest one for the rutile phase. We can judge the change in phase composition by the position as well as relative intensity of peaks. When the volume of HNO₃ medium gained, the relative intensity of band at 445 cm⁻¹ and 612 cm⁻¹ for R phase become weaker. This can be explained by the decrease of weight fraction of R. Both of the changes in relative intensity and position of Raman bands are in accordance with those of XRD patterns, which further proved the evolution of phase composition by altering the volume of HNO₃ solution in the crystallization step.

Changes in morphology and particle size simultaneously bring about the difference in specific surface area of samples. The values can be calculated from nitrogen adsorption-desorption isotherms (Fig. 4 and Table 1). Compared with 1D nanostructures, 0D nanostructures have higher surface-to-volume ratio, which means larger surface area. Due to the lower surface-to-volume ratio of 1D Nr, S1 possesses the lowest surface area as 111 m²/g, which is much smaller than that of S2 to S4. Surface area of S4 reaches 215 m²/g, which is almost twice as large as that of S1 because of the Np's high surface-to-volume ratio. From S1 to S4, the ratio of Np gradually increases and the crystal size decreases, both leading to the increase of surface area. Thus we conclude that the phase composition, morphology, and surface area can be facily controlled through adjusting the volume of HNO₃ medium. These results are given and compared in Table 1. Overall, the tendency is that adding more HNO₃ solution during crystallization step is in favour of forming crystals with larger proportion of anatase Np and larger surface area.

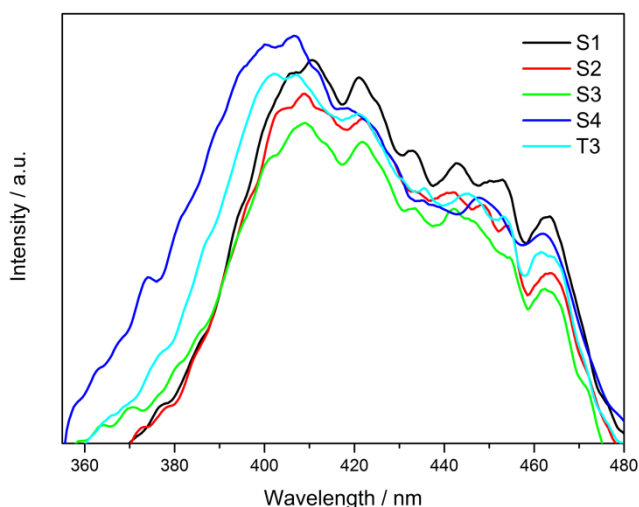


Figure 6 PL spectra of S-series samples and one of T-series samples, which has similar phase composition to S3.

Effect of NaOH treatment on morphology and specific surface area

Since morphology will influence the surface area and the photocatalytic performance, comparisons of these properties between 0D/1D composite structure and pure 0D structure should be considered. Previous study evidenced that NaOH treatment has little influence on the phase composition of TiO₂ composite but is essential to the fabrication of R nanorods via such soft-chemical strategy.¹⁶ That is to say, pure 0D products with similar phase composition can be synthesized with no NaOH treatment, which are labeled as T-series samples (from T1 to T3). In this regard, the properties of T-series samples (not treating by NaOH) are analyzed and compared with S-series samples (treating by NaOH).

According to XRD patterns in Fig. S1 in supporting information, the phase composition of T-series samples is calculated and the results are given in Table 1. Through adjusting the volume of HNO₃ solution, samples T1-T3 are controlled to contain the similar weight fractions of A and R to samples S1-S3, respectively. The results also reflect that both A and R phase formed whether the hydrolysate was treated with NaOH or not, and the phase transition occurred following the same regulation. When taking sample T3 as an example, it consists of 71% of A and 29% of R, which is very close to that of sample S3 (70% of A and 30% of R). Differently, the TEM image reveals that T3 presents no obvious 1D structure (Fig. 5). Besides, NaOH treatment has some effect on the size of 0D particles. As shown in Fig. 3, the main features of the Raman spectrum of sample T3 are very similar to those of sample S3. Using the Photon Confinement Model, the overall half-width at half-height of Raman band is proportional to the inverse of the grain size.⁴² It is clear that the Raman bands become asymmetric broadening and the intensities decrease in sample T3, suggesting the decrease of crystal size in contrast to the samples with NaOH treatment. This is consistent with XRD calculation. Because of higher surface-to-volume ratio of 0D Np, T1, T2 and T3 possess the higher surface area than S1, S2 and S3, respectively. For instance, the surface area of T3 reaches as high as 235 m²/g (Fig. S2 and Table 1). In addition, we find the same trend in S_{BET} values changing of T-

series products with phase composition, which is also attributed to the similar effect of reacting space (i.e. volume of HNO₃ medium) on the oriented arrangement of structural units and the phase transition from A to R. Therefore, NaOH treatment before acid peptization negligibly affects the phase composition but significantly affects the morphology, surface area, and the resulted photocatalytic activity. S-series and T-series samples can be used to explain the difference between 0D/1D composite structure and pure 0D structure when using TiO₂ as photocatalysts.

Phase composition and morphology on the charge carriers separation

In general, photocatalytic processes involve the excitation, bulk diffusion, surface transfer of photoinduced charge carriers, and radical chain reaction. Only the separated carriers will participate in the following radical chain reaction. For single component TiO₂, most of the photogenerated electron-hole (e⁻-h⁺) pairs inevitably recombine at bulk or at surface trapping sites, with the release of photons and heat, resulting in PL spectra. Hence PL spectra can be used to compare the recombination level of photogenerated e⁻-h⁺ pairs within different photocatalysts.⁴³⁻⁴⁵

The PL spectra of S-series and T-series samples exhibit the similar emission bands for all TiO₂ samples, indicating the similar defect level for A and R phase (Fig. 6 and Fig. S3). In comparison to single component TiO₂ (S1 and S4), the lower recombination rate is observed in A/R heterogeneous system such as S2 or S3. The same result is also discovered among T1, T2 and T3. For single component TiO₂, the e⁻-h⁺ recombination may be grouped into two categories: bulk recombination and surface recombination. Bulk recombination is a dominant process in well-crystallized large TiO₂ particles. When the particle size was reduced to around 10 nm, the average migration time of e⁻ and h⁺ from the particle bulk to the surface is very fast, so the surface recombination become an important process.^{46,47} In heterogeneous system, the difference in conduction band energy of A and R phase will act as a driving force for electrons transport between their contacting surfaces and thus improve the surface charge separation to some extent. More importantly, the long-shaped crystals are constructed of isoelectronic materials that permit easy electron transport along the long direction. The introduction of 1D TiO₂ nanorods instead of 0D nanoparticles will result in the decreased number of contact barriers between crystals, which usually forms grain boundaries acting as electron traps.^{26,48-52} Therefore, the charge carrier separation is more efficient in A/R heterogeneous nanostructure containing 1D TiO₂ nanorods (S3) than that consisting of pure 0D nanoparticles (T3).

Photocatalytic activity

The influence of phase composition, morphology, and specific surface area on the photocatalytic performance over TiO₂ samples is studied via degrading a series of organic dyes under UV light irradiation (Fig. 7). Before degradation experiments, the rates of adsorption progress in samples are also tested (Fig. 7a). The adsorption capacity increases from S1 to S4 in S-series samples due to the same trend in specific surface area. Particles with large surface area usually have more active sites to absorb organic molecules for photodegradation. Sample S1 with pure R phase exhibits the poorest photoreactivity of all samples (Fig. 7b,c),

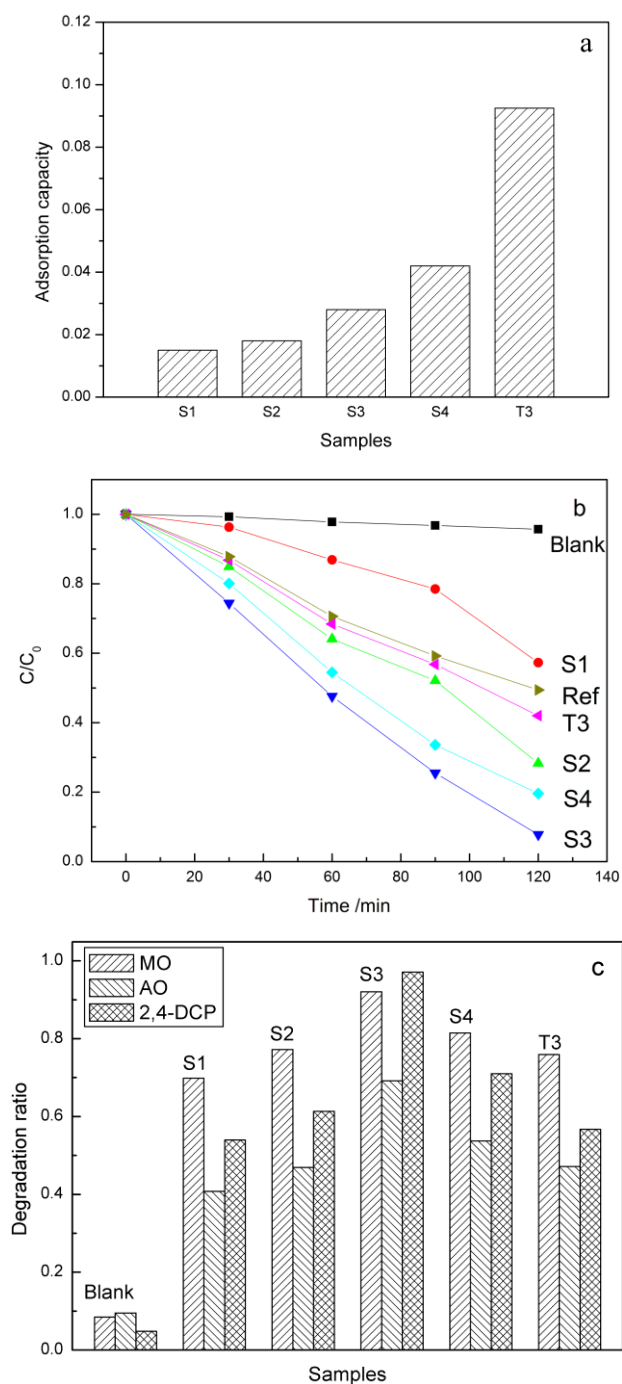


Figure 7 (a) Adsorption capacity of TiO₂ samples by recording changes in MB concentration before and after continuous stirring in the darkness for 40 min. (b) Evolution of MB concentration versus UV irradiation time in the absence of photocatalysts (Blank) and in the presence of TiO₂ samples. "Ref" is the reference sample, anatase nanoparticles with an average particle size of ~20 nm. (c) Comparison of photocatalytic activities among TiO₂ photocatalysts under UV irradiation (100 min for MO and 2,4-DCP, 200 min for AO).

which is probably due to the lower adsorption affinity for organic molecules and a higher recombination rate than A phase besides the lowest surface area.⁵⁻⁷ From S1 to S4, both S_{BET} value and adsorption capacity increase stepwise, however, the photocatalytic activity increases with A content at the beginning, and then turn to a downtrend when the transition to R phase is

further inhibited. The relatively optimal performance is obtained with sample S3, consisting of 70% of A and 30% of R. That is, the highest surface area in S4 does not endow it the best reactivity. Bechstein and Besenbacher et al correlated the photoreactivity to the A-to-R ratio from a wide A content range of 0~86%. They highlighted a region of A content from 40% to 80%, which displayed a sufficient synergetic effect in contrast to other regions.⁸ The limited activity is observed in rutile-dominant composite like sample S2, even much lower than that of S4 with almost pure A phase, which is probably due to the combined effect of lower surface area and insufficient amount of A. In sample S4, the amount of R is insufficient to assist in such synergetic effect.

A lively discussion on the exact cause or process of such synergism between A and R phases has appeared in the literatures. The bandgap of TiO₂ crystal is 3.20 eV for anatase and 3.03 eV for rutile. Since Kavan et al proposed the conduction band edge of A 0.2 eV higher than that of R according to electrochemical impedance analysis,⁵³ it has been generally accepted that the photogenerated e⁻ transfers from A to R and the h⁺ transfers from R to A at their interface, which was also supported by several other experiments.¹⁰⁻¹² Consequently, the e⁻ in the conduction band of R is consumed by the reduction of O₂, while the h⁺ in the valence band of A oxidizes organic substrates, leading to efficient charge separation. Some alternative measurements, such as photoemission electron microscopy and electron paramagnetic resonance, have revealed that e⁻ flows from R into A, while h⁺ moves in the opposite direction.⁵⁴⁻⁵⁶ Most recently, Scanlon et al revised the band model of A and R with a staggered alignment of ~0.4 eV. They demonstrated that e⁻ flowing from R to A was attributed to the higher electron affinity of A than R. The alignment of 0.4 eV contributes to lowering the effective bandgap of composite materials and facilitating efficient e⁻-h⁺ separation.⁵⁷ There is other explanation for less active R TiO₂ from Xu's group that R has a lower affinity to O₂ than A in water. They reported that A not only acted as a photocatalyst but also functioned as an oxygen source for supplying R in mixed phase. In this way, the adsorbed O₂ on A phase diffused onto the R sites to scavenge the conduction band electron of R, resulting in the increase of "intrinsic" photoactivity of TiO₂.⁵⁸ Although the controversy in roles of A and R always exists, it seems plausible to assume that A and R phase function as two different semiconductors in the composite structure since they have some different properties, whatever the band model, electron or oxygen affinity. Each of these proposed differences could act as a driving force for the charge carrier separation and the resulted improvement of photoactivity in A/R composite, which can be evidenced by measurements of PL spectra and photocatalytic experiments. What is distinguished from other composite systems is that such composite is comprised of TiO₂ polymorph, having the same structure unit and being able to achieve in the same reaction system.

For T-series samples, T3 possesses the highest value of S_{BET} and also exhibit the strongest adsorption capacity, implying that higher surface area brings about the obvious increase in adsorption capacity even if samples are prepared from different process. However, T3 does not display the expectedly high reactivity as S3 for dye decomposition though both of them are

composed of A-to-R ratio as 7:3 or so. For 0D structure like T3, decrease of particle size brings about the increased surface area and the reduced bulk recombination, however, e^-h^+ pairs may quickly reach the surface and undergo rapid surface recombination because of the abundant surface trapping sites.⁴⁷ In 1D TiO₂ nanorods, the delocalized carriers are free to move throughout the length of the crystal. This could partially compensate for the occurrence of surface trap states and ensure a more efficient charge separation.²⁶ Compared with pure 0D structure, the drawbacks of 0D/1D composite arising from larger particle size and lower surface-to-volume ratio are significantly offset by the reduced e^-h^+ recombination probability.

Conclusions

In summary, we have synthesized a series of TiO₂ samples from a facile soft-chemical system. Through simply altering the volume of acid peptizer, TiO₂ nanomaterials possess varied phase composition, morphology, specific surface area, but otherwise identical physical/chemical properties. First, the anatase-to-rutile phase transition is hindered by the increase of acid volume due to the limited orientational aggregation. Second, NaOH treatment is essential to the fabrication of 0D/1D heterogenous structure but has little influence on the phase composition. Third, due to the higher surface-to-volume ratio of 0D particles, the specific surface area increases with the decrease of 1D rutile content and reaches as high as 235 m²/g in pure 0D structure.

In anatase/rutile composite, the different properties between them favor the charge carrier separation in case of electrons or oxygen flowing from one to another. Compared with single structure, the 0D/1D TiO₂ heterogenous structure combines the merits of higher surface-to-volume ratio of 0D particles with the lower carriers recombination of 1D nanorods. As expected, the photocatalytic measurement shows that the superior performance for dye decomposition is achieved in 0D/1D composite with anatase-to-rutile ratio as 7:3 and S_{BET} value as 184 m²/g. These results would be important in designing highly active TiO₂-based photocatalysts for application in environmental purification and energy conversion.

Acknowledgements

This work is supported by the National Natural Science Foundation of China (21001037, 21071037, and 91122002), the Special Fund of Harbin Technological Innovation talent (2013RFLXJ011), and the Research Fund for Talent Introduction of Huazhong University of Science and Technology.

Notes and references

^a School of Chemistry and Chemical Engineering, Huazhong University of Science and Technology, 1037 Luoyu Road, Wuhan 430074, China.

^b Department of Chemistry, Harbin Institute of Technology, 92 West Dazhi Street, Harbin 150001, China.

Email: jingyu.wang@163.com; hanxj63@yahoo.com.cn.

- H.H. Chen, C.E. Nanayakkara and V.H. Grassia, *Chem. Rev.*, 2012, **112**, 5919.
- T.L. Thompson and J.T. Yates, *Chem. Rev.*, 2006, **106**, 4428.
- A. Fujishima, K. Hashimoto and H. Watanabe, *TiO₂ photocatalysis: fundamentals and applications*, BKC Inc, Tokyo, 1999.
- A. Fujishima and K. Honda, *Nature* (London), 1972, **238**, 37.

- U. Stafford, K.A. Gray, P.V. Kamat and A. Varma, *Chem. Phys. Lett.*, 1993, **205**, 55.
- D.C. Hurum, A.G. Agrios, K.A. Gray, T. Rajh and M.C. Thurnauer, *J. Phys. Chem. B*, 2003, **107**, 4545.
- A.L. Linsebigler, G. Lu and J.T. Yates, *Chem. Rev.*, 1995, **95**, 735.
- R. Su, R. Bechstein, L. So, R.T. Vang, M. Sillassen, B. Ebsjornsson, A. Palmqvist and F. Besenbacher, *J. Phys. Chem. C*, 2011, **115**, 24287.
- S.X. Li, J. Chen, F.Y. Zheng, Y.C. Li and F.Y. Huang, *Nanoscale*, 2013, **5**, 12150.
- D.L. Jiang, S.Q. Zhang and H.J. Zhao, *Environ. Sci. Technol.*, 2007, **41**, 303.
- T. Kawahara, T. Ozawa, M. Iwasaki, H. Tada and S. Ito, *J. Colloid Interface Sci.*, 2003, **267**, 377.
- T. Kawahara, Y. Konishi, H. Tada, N. Tohge, J. Nishii and S. Ito, *Angew. Chem. Int. Ed.*, 2002, **114**, 2811.
- Z.B. Rui, S.R. Wu, C. Peng and H.B. Ji, *Chem. Eng. J.*, 2014, **243**, 254.
- H. Kaper, F. Endres, I. Djerdj, M. Antonietti, B. M. Smarsly, J. Maier and Y.S. Hu, *Small*, 2007, **3**, 1753.
- J.Y. Wang, X.J. Han, C. Liu, W. Zhang, R.X. Cai and Z.H. Liu, *Cryst. Growth Des.*, 2010, **10**, 2185.
- J.Y. Wang, X.J. Han, W. Zhang, Z.K. He, C. Wang, R.X. Cai and Z.H. Liu, *CrystEngComm*, 2009, **11**, 564.
- L.Y. Hu, J.Y. Wang, J.X. Zhang, Q.Y. Zhang and Z.H. Liu, *RSC Adv.*, 2014, **4**, 420.
- X.J. Shen, J.L. Zhang and B.Z. Tian, *J. Hazard. Mater.*, 2011, **192**, 651.
- Y.K. Kho, A. Iwase, W. Y. Teoh, L. Madler, A. Kudo and R. Amal, *J. Phys. Chem. C*, 2010, **114**, 2821-2829.
- G.H. Li, C.P. Richter, R.L. Milot, L. Cai, C.A. Schmuttenmaer, R.H. Crabtree, G.W. Brudvig and V.S. Batista, *Dalton T.*, 2009, **45**, 10078.
- M.C. Yan, F. Chen, J.L. Zhang and M. Anpo, *J. Phys. Chem. B*, 2005, **109**, 8673.
- C.Y. Wu, Y.H. Yue, X.Y. Deng, W.M. Hua and Z. Gao, *Catal. Today*, 2004, **93-95**, 863.
- L. Pan, H. Huang, C.K. Lim, Q.Y. Hong, M.S. Tse and O.K. Tan, *RSC Adv.*, 2013, **3**, 3566.
- X. Wu, G.Q. Lu and L.Z. Wang, *Energy Environ. Sci.*, 2011, **4**, 3565.
- C.H. Wang, X. T. Zhang, C.L. Shao, Y.L. Zhang, J.K. Yang, P.P. Sun, X.P. Liu, H. Liu, Y.C. Liu, T.F. Xie and D.J. Wang, *J. Colloid Interface Sci.*, 2011, **363**, 157.
- P.D. Cozzoli, A. Kornowski and H. Weller, *J. Am. Chem. Soc.*, 2003, **125**, 14539.
- H. Kominami, S. Murakami, J. Kato, Y. Kera and B. Ohtani, *J. Phys. Chem. B*, 2002, **106**, 10501.
- G. Tian, H. Fu, L. Jing, B. Xin and K. Pan, *J. Phys. Chem. C*, 2008, **112**, 3083.
- C.H. Chen, Q.W. Liu, S.M. Gao, K. Li, H. Xu, Z.Z. Lou, B.B. Huang and Y. Dai, *RSC Adv.*, 2014, **4**, 12098.
- J.B. Joo, Q. Zhang, M. Dahl, I. Lee, J. Goebel, F. Zaera and Y. Yin, *Energy Environ. Sci.*, 2012, **5**, 6321.
- A. Bojinova, R. Kralchevska, I. Poullos and C. Dushkin, *Mater. Chem. Phys.*, 2007, **106**, 187.
- R.K. Wahi, W.W. Yu, Y.P. Liu, M.L. Mejia, J.C. Falkner, W. Nolte, and V.L. Colvin, *J. Mol. Catal. A*, 2005, **242**, 48.
- Q.A. Xu, Y. Ma, J. Zhang, X.L. Wang, Z.C. Feng and C. Li, *J. Catal.*, 2011, **278**, 329.
- R.G. Nair, S. Paul and S.K. Samdarshi, *Sol. Energy Mater. Sol. Cells*, 2011, **95**, 1901.
- D. Su, J.Y. Wang, Y.P. Tang, C. Liu, L.F. Liu and X.J. Han, *Chem. Commun.*, 2011, **47**, 4231.
- C.-C. Wang and J.Y. Ying, *Chem. Mater.*, 1999, **11**, 3113.
- M.C. Yan, F. Chen, J.L. Zhang, and M. Anpo, *J. Phys. Chem. B*, 2005, **109**, 8673.
- L.A. Gu, J.Y. Wang, H. Cheng, Y.C. Du and X.J. Han, *Chem. Commun.*, 2012, **48**, 6978.
- R.L. Penn and J.F. Banfield, *Am. Mineral.*, 1999, **84**, 871.
- H.Z. Zhang and J.F. Banfield, *J. Phys. Chem. B*, 2000, **104**, 3481.
- J. Zhang, M.J. Li, Z.C. Feng, J. Chen and C. Li, *J. Phys. Chem. B*, 2006, **110**, 927.

- 42 G. Gouadec and P. Colomban, *Prog. Cryst. Growth Charact. Mater.*, 2007, **53**, 1.
- 43 J.C. Yu, J.G. Yu, W.K. Ho, Z.T. Jiang and L.Z. Zhang, *Chem. Mater.*, 2002, **14**, 3808.
- 5 44 Y.Q. Cao, Y.L. Yu, P. Zhang, L.L. Zhang, T. He and Y.A. Cao, *Sep. Purif. Technol.*, 2013, **104**, 256.
- 45 W. Teng, X.Y. Li, Q.D. Zhao and G.H. Chen, *J. Mater. Chem. A*, 2013, **1**, 9060.
- 46 N. Serpone, D. Lawless, R. Khairlutdinov and E. Pelizzetti, *J. Phys. Chem.*, 1995, **99**, 16655.
- 10 47 Z.B. Zhang, C.C. Wang, R. Zakaria and J.Y. Ying, *J. Phys. Chem. B*, 1998, **102**, 10871.
- 48 J.T. Jiu, S. Isoda, F.M. Wang and M. Adachi, *J. Phys. Chem. B*, 2006, **110**, 2087.
- 15 49 Z.R. Tang, X. Yin, Y.H. Zhang and Y.J. Xu, *RSC Adv.*, 2013, **3**, 5956.
- 50 Z.R. Tang, Y. Zhang and Y.J. Xu, *ACS Appl. Mater. Interfaces*, 2012, **4**, 1512.
- 51 K. Zhu, N.R. Neale, A. Miedaner and A.J. Frank, *Nano Lett.*, 2007, **7**, 69.
- 20 52 A.B.F. Martinson, J.E. McGarrah, M.O.K. Parpia and J.T. Hupp, *Phys. Chem. Chem. Phys.*, 2006, **8**, 4655.
- 53 L. Kavan, M. Gratzel, S.E. Gilbert, C. Klemenz and H.J. Scheel, *J. Am. Chem. Soc.*, 1996, **118**, 6716.
- 54 G. Xiong, R. Shao, T.C. Droubay, A.G. Joly, K.M. Beck, S.A. Chambers and W.P. Hess, *Adv. Funct. Mater.*, 2007, **17**, 2133.
- 25 55 D.C. Hurum, A.G. Agrios, S.E. Crist, K.A. Gray, T. Rajh and M.C. Thurnauer, *J. Electron Spectrosc.*, 2006, **150**, 155.
- 56 D.C. Hurum, A.G. Agrios, K.A. Gray, T. Rajh and M.C. Thurnauer, *J. Phys. Chem. B*, 2003, **107**, 4545.
- 30 57 D.O. Scanlon, C.W. Dunnill, J. Buckeridge, S.A. Shevlin, A.J. Logsdail, S.M. Woodley, C.R.A. Catlow, M.J. Powell, R.G. Palgrave, I.P. Parkin, G.W. Watson, T.W. Keal, P. Sherwood, A. Walsh and A. A. Sokol, *Nat. Mater.*, 2013, **12**, 798.
- 58 S. Cong and Y.M. Xu, *J. Phys. Chem. C*, 2011, **115**, 21161.

35